ISSN: 1410-8917
e-ISSN: 2597-9914

Jurnal Kimia Sains dan Aplikasi 28 (9) (2025): 502-511

Jurnal Kimia Sains dan Aplikasi
Journal of Scientific and Applied Chemistry

Journal homepage: http://ejournal.undip.ac.id/index.php/ksa

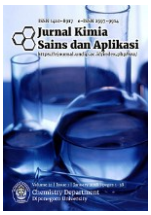

Biosynthesis of ZnO Nanoparticles from *Cnidoscolus aconitifolius* Leaf Extract: Structure, Morphology, and Photocatalytic Performance for Methylene Blue and Methyl Orange Degradation by UV Light Irradiation

Sri Wahyu Suciyati [1,*], Anisatul Mahmudah [1], Lusia Prastica [1], Ayu Aprilia [1]

[1] Department of Physics, University of Lampung, Bandar Lampung-35145, Indonesia

* Corresponding author: sri.wahyu@fmipa.unila.ac.id

https://doi.org/10.14710/jksa.28.9.502-511

Article Info

Article history:

Received: 17th July 2025
Revised: 03rd November 2025
Accepted: 25th November 2025
Online: 08th December 2025

Keywords:
Cnidoscolus aconitifolius; ZnO NPs; biosynthesis; photocatalytic

Abstract

Zinc oxide nanoparticles (ZnO NPs) were produced via an environmentally friendly approach using *Cnidoscolus aconitifolius* leaf extract and subsequently heat-treated at 250°C. The presence of Zn–O vibrations and organic functional groups in the extract was verified by FTIR analysis, while XRD data revealed a wurtzite structure with a mean crystallite dimension of 17.64 nm. SEM images mainly showed round-shaped particles with a band gap energy of 3.29 eV. Assessments of photocatalytic capability indicated substantial degradation of methylene blue (MB, reaching 92.96%), in contrast to diminished degradation of methyl orange (MO, registering 43.93%). This improved effectiveness was attributed to the combined favorable effects of concurrent photocatalytic processes. The kinetic evaluation followed a pseudo-second-order model, yielding rate constants of 0.38 min^{-1} for MB and 0.064 min^{-1} for MO. Overall, the green-synthesized ZnO NPs calcined at 250°C exhibit excellent photocatalytic activity, particularly for the degradation of MB.

1. Introduction

Nanoparticles are nanostructured materials with one dimension measuring 1–100 nm [1]. Nanoscale particles' physical, chemical, and biological properties are increasing compared to bulk materials. Metal oxide materials, such as zinc oxide (ZnO), have been frequently synthesized due to their wide range of applications in various fields [2]. Conventionally, ZnO nanoparticle synthesis is carried out by physical and chemical processes. However, this method is considered inefficient because it is expensive, requires high energy, and involves toxic and dangerous chemicals. Chemicals such as sodium borohydride, ethylene glycol, and dimethylformamide can be used as reducing agents, but they can also produce environmental pollution [3, 4].

Biosynthesis, also known as green synthesis, has been developed as an alternative to minimize the use of chemical reducing agents. Biosynthesis is a synthesis method that utilizes plants and microorganisms as reducing and capping agents in the metal oxide synthesis process [5, 6]. The characteristics of plants that contain secondary metabolites, such as flavonoids, polyphenols, terpenoids, phenolic acids, and tannins, can be utilized to reduce and stabilize nanoparticle formation [7]. The green synthesis of ZnO nanoparticles has been widely developed in various plants and applications. Rambutan peel extract for medical applications [8], mango leaf extract for antioxidants [9] and photocatalysis [10], jujube fruit extract as a photocatalyst for color degradation [11], carica papaya leaf extract for antibacterial and increasing the hydrophobic properties of cotton fabrics [12], papaya peel extract as a photocatalyst for the degradation of oil spills [13], *Crescentia cujete* L. leaf extract as a photocatalyst for the degradation of methylene blue [14].

Cnidoscolus aconitifolius is a relatively new type of vegetable plant known in Indonesia. This plant is also known as "Japanese papaya", which originates from Central America and is known as chaya in its place of origin [15]. Based on Kuri-García *et al.* [16], *Cnidoscolus*

aconitifolius leaf extract contains many phytochemical compounds used as antioxidants and anti-diabetics. With the abundance of these compounds, *Cnidoscolus aconitifolius* leaves have the potential to be used as a substitute for reducing and capping agents in the metal oxide synthesis process. The main phytochemicals present in plants are flavones, terpenoids, sugars, ketones, aldehydes, carboxylic acids, and amides, which are responsible for the bioreduction of nanoparticles [17].

Although *Cnidoscolus aconitifolius* leaf extract was utilized in the green production of ZnO NPs by Suciyati *et al.* [18] in earlier studies, its photocatalytic activity was not optimized. By calcining the ZnO NPs sample, our work advanced the earlier technique. It is anticipated that the formation of ZnO NPs would be maximized. FTIR, XRD, SEM, UV-DRS, and UV-Vis spectroscopy were used to characterize the outcomes of ZnO NPs synthesis. The formation phases and optical characteristics that enhance ZnO NPs' photocatalytic activity were the main focus of the investigation. Methylene blue (MB) and methyl orange (MO) degradation were used to assess the photocatalytic qualities of the ZnO NPs photocatalysts at different masses.

2. Experimental

2.1. Materials

Cnidoscolus aconitifolius leaf, ethanol (C_2H_6) (97%, Merck), sodium hydroxide (NaOH) (75%, Merck), zinc nitrate hexahydrate ($Zn(NO_3)_2.6H_2O$) (95%, Merck), methylene blue, methyl orange dyes, and deionized water (DI water). All materials were used without further purification. Ethanol and deionized water were used to neutralize the solution and as the solvent, respectively.

2.2. Preparation of *Cnidoscolus aconitifolius* Leaves Extract

Cnidoscolus aconitifolius fresh leaves were gathered in Bandar Lampung, Indonesia. The first step in the extraction procedure was to rinse the *Cnidoscolus aconitifolius* leaves under tap water to remove any dust, then sun-dried. After drying, 10 g of the leaves were weighed and chopped into small pieces using a blender. To create a 5% w/v solution, the crushed leaves were combined with 200 mL of demineralized water. To make a pallid green extract, the resultant liquid was heated to 80°C while being stirred, and then sieved through filter paper. To use it as a restricting agent in the manufacture of ZnO NPs, the extract was finally stored in a refrigerator. The dark green, finger-like leaves of *Cnidoscolus aconitifolius* used in this study are shown in Figure 1(a). To improve the extraction of phytochemical substances, *Cnidoscolus aconitifolius* leaves were chopped, as seen in Figure 1(b). To avoid potential structural damage to the phytochemical components, the extraction procedure was carried out at a temperature ≤ 80°C. The extraction of *Cnidoscolus aconitifolius*, which produces golden brown solutions, is shown in Figure 1(c).

2.3. Biosynthesis of ZnO NPs

In the current study, ZnO NPs were synthesized using *Cnidoscolus aconitifolius* (chaya) leaf extract as the biological material for reduction and stabilization, following the environmentally friendly synthesis method reported by Suciyati *et al.* [18], which also utilized *Cnidoscolus aconitifolius* extract. Three solutions (S-1, S-2, and S-3) were prepared. Solution S-1 was obtained by dissolving 5 g of zinc nitrate hexahydrate in 100 mL of deionized water and stirring for one hour at 27°C. Solution S-2 consisted of 50 mL of *Cnidoscolus aconitifolius* leaf extract, while S-3 was prepared by mixing 50 mL of deionized water with 0.7 M NaOH. Solutions S-1 and S-2 were then combined and stirred at 80°C for 15 minutes before cooling to 27°C. Once both mixtures reached room temperature, S-3 was added dropwise under continuous stirring for three hours until the solution turned dark yellow, indicating ZnO NP formation. The mixture was centrifuged at 4000 rpm for 15 minutes, and the resulting precipitate was washed alternately with ethanol and bidistilled water. The precipitate was then dried at 80°C, calcined at 250°C for 2 hours, and finally ground with an agate mortar to obtain the ZnO NPs powder (ZnO-b).

To clarify the sample designation, two types of ZnO NPs were prepared. The first sample, ZnO-a, was synthesized following the method reported in the reference [18] and was not subjected to any further heating. The second sample, ZnO-b, was produced using the same procedure but was additionally heated at 250°C for two hours. This post-treatment was applied to evaluate the effect of heat on the crystal structure, morphology, and optical properties of the green-synthesized ZnO. Both samples were prepared and characterized under identical experimental conditions to enable a fair comparison.

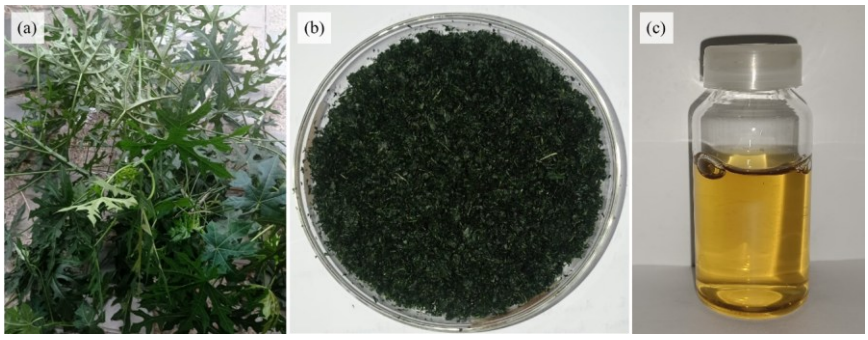

Figure 1. *Cnidoscolus aconitifolius*: (a) fresh leaves, (b) crushed, (c) extract

2.4. Characterizations

Fourier Transform Infrared (FTIR) spectroscopy (PerkinElmer Spectrum IR Version 10.6.1) was used to identify the functional groups of the ZnO NPs. The crystalline structure was analyzed using XRD (Panalytical X'Pert Pro diffractometer) operated at 30 kV and 50 mA with CuKα radiation (λ = 1.5406 Å) and a step size of 0.02°. Rotation goniometry was used to record data in the 2θ range of 3° to 90°. The optical band gap was measured using the SPECORD 210 PLUS spectrophotometer (plate number: 223F1936C) and the UV-Vis DRS. Samples were examined for the degradation of MB and MO dyes, with a focus on photocatalytic applications. A Shimadzu CARY 100 spectrophotometer (200–800 nm) was used to monitor photocatalytic activity. MB and MO solutions (10 ppm, ~100 mL) were prepared, and 0.1 g of photocatalyst was added to each. The mixtures were then irradiated with UV light for 90 minutes at 30-minute intervals.

3. Results and Discussion

3.1. Phytochemicals Screening and FTIR Spectra Analysis

The secondary metabolite content of *Cnidoscolus aconitifolius* leaf extract was tested using a qualitative method based on color changes that occur when the extract reacts with specific reagents. The results of this phytochemical screening are shown in Table 1, where the observed color changes confirm the presence of secondary metabolites in the leaf extract [19]. These phytochemicals support the use of *Cnidoscolus aconitifolius* extract as a capping, stabilizing, and reducing agent in the synthesis of metal-based materials, including nanoparticles and metal oxides [20].

In addition to the phytochemical screening test, the certainty of the presence of metabolite compounds is assured by the results of FTIR characterization (Figure 2). The detected transmittance peaks confirm the presence of flavonoids, phenolics, alkaloids, tannins, and steroids in the leaf extract of *Cnidoscolus aconitifolius.* Table 1 shows the FTIR-phytochemical correlation for both the leaf extract (Chaya LE) and the ZnO NPs. The agreement between the phytochemical screening results and the FTIR absorption bands confirms the consistency of the observed functional groups and secondary metabolites.

FTIR spectra of ZnO NPs are shown in Figure 2, covering the absorption range of 400-4000 cm^{-1}. Functional groups and their appearance in the IR wave spectrum are stated in Table 1. Phytochemical screening confirmed the presence of alkaloids, flavonoids, tannins, phenolics, and steroids, which aligns with the FTIR absorption peaks observed in the 1200–3350 cm^{-1} region (C–O, C–N, O–H, N–H) and the 1500–1900 cm^{-1} region (C=O or C=C), which are typically associated with with phenolic, flavonoid, and amine-containing compounds. The presence of hydroxyl (O–H), carbonyl (C=O), and amine (C–N or N–H) groups is known to act as reducing and stabilizing agents during the green synthesis of ZnO NPs. This is consistent with previous plant-mediated ZnO synthesis studies, which report similar FTIR features and interaction mechanisms between phenolic/amine groups and Zn^{2+} ions during nanoparticle formation [20, 21].

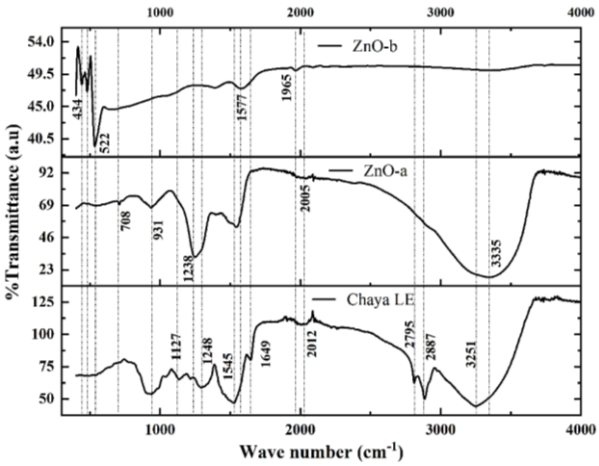

Figure 2. FTIR spectra of ZnO NPs obtained from *Cnidoscolus aconitifolius* leaf extract. Reference patterns of ZnO-a and Chaya LE were taken from Suciyati *et al.* [18]

Table 1. Correlation between phytochemical screening and FTIR wavenumbers of Chaya LE and ZnO NPs

Secondary metabolites	Result (color change)	Wavenumber (cm^{-1})	Type of spectrum/vibration	Functional group interpretation
Alkaloids (3 tests)	White precipitate (+) Orange (+) Brown (+)	1127, 1248, 1518-1545	C-N stretching, N- H, and N-O vibration	Amine and nitro groups indicate alkaloid presence
Flavonoids	Yellowish (+)	1649, 3251-3335	C=O and O-H stretching	Carbonyl and hydroxyl groups supporting flavonoids presence
Tannins	Greenish (+)	1238, 3335	C-O and O-H stretching	Phenolic compounds with hydroxyl and ether groups
Phenolics	Greenish (+)	1238, 3251	C-O and O-H stretching	Free phenolic and aromatic alcohol groups
Saponins	No foam (-)	-	-	Not detected in phytochemical and FTIR tests
Steroids	Green (+)	1649–1891, 1965–2012	C=C and C–H bending	Double bond (C=C) and C–H bending are typical of the steroid skeleton
Aromatic compounds/ZnO		410, 434, 522, 708, 931	Zn–O stretching and C–H aromatic	Indicates ZnO NPs formation and residual organic compounds from the leaf extract

Evidence of ZnO nanoparticle formation in the composite sample is confirmed by a strong absorption band at 410–522 cm^{-1}, corresponding to the stretching vibration of the Zn–O bond. This is consistent with numerous reports on the biosynthesis of ZnO using plant extracts, where the Zn–O peak typically appears around 400–500 cm^{-1}, and organic peaks attached to the nanoparticle surface indicate capping by phytoconstituents (phenols, flavonoids, proteins/amides) [20, 22]. The peaks at 708 and 931 cm^{-1} are attributed to the functional group of the aromatic ring, which is a characteristic feature of organic compounds in *Cnidoscolus aconitifolius* leaves [18, 22, 23]. This group is confirmed in a report by Soto-Robles *et al.* [24], which shows the influence of flavonoids, phenolics, and other phytochemical compounds in leaf extract (LE) on reducing particle size and stabilizing zinc salts in aqueous media. Therefore, the combination of phytochemical and FTIR results not only validates the identification of bioactive compound classes but also elucidates their mechanistic roles in the reduction, nucleation, and stabilization of ZnO NPs within the framework of green synthesis [25].

The broad and intense absorption peaks at 3335 and 3251 cm^{-1} correspond to O-H stretching [26] and N-H vibrations in Chaya LE [27, 28], which causes water absorption on the ZnO surface. This is corroborated by another report [29], which correlated the shift in the position and peak intensity of the spectral peaks of leaf extract samples with the interactions of the flavonoid and phenol groups in the ZnO NPs spectra. Additionally, it was mentioned that the extract's functional groups transfer electrons, which can reduce zinc ions and, eventually, zinc nanoparticles (Zn^0). The FTIR spectra of ZnO NPs (Figure 2) showed a shift in peak and intensity from 3251 (Chaya LE) to 3335 cm^{-1} (ZnO-a) and almost disappeared in ZnO-b, indicating that the main biomolecules of *Cnidoscolus aconitifolius* leaves were restricted or bound to the ZnO NPs surface. In addition, the shift of this peak in ZnO NPs was caused by O-H phenol groups and -NH_2 stretching vibrations. The functional groups in the leaf extract assist the reduction mechanism of zinc ions to form zinc nanoparticles through electron donation [29]. During calcination, the ZnO-b sample lost water from its surface, as evidenced by the FTIR spectrum (at 3335 cm^{-1}).

3.2. XRD Spectra

XRD diffractogram (Figure 3) shows the synthesized ZnO NPs diffraction graph from *Cnidoscolus aconitifolius* leaf extract. Qualitative analysis revealed that this sample is close to the standard ZnO database (JCPDS no. 01-089-0510), where the 11 diffraction peaks correspond to those of the synthesized sample. The diffraction peak at 2θ is the formation of the hexagonal wurtzite structure. Figure 3 shows that the synthesized nanoparticles ZnO-a and ZnO-b have a hexagonal wurtzite structure, according to the JCPDS database No. 01-089-0510. The crystal structure, space groups, and parameters of the lattice of ZnO-b are shown in Table 2. The crystallite size and the unit cell volume of the hexagonal structure were calculated using Equations (1) and (2) [26].

$$D = \frac{0.9\lambda}{B\cos\theta} \quad (1)$$

$$V = 0.866\, a^2 c \quad (2)$$

Where, D = crystallite size (nm), λ = 1.5406 (Å), B = full width at half maximum (rad), θ = diffraction angles (deg), a,c = parameters of lattice (nm). By calculating the XRD data from 10 diffraction peaks, the average value of the crystallite size of the synthesized sample (Equation 1) is 17.635 nm (ZnO-b NPs). The unit cell volume is 5.5077 nm^3 (55.077 $Å^3$). The tiny crystallite size suggests a high surface-area-to-volume ratio, which may enhance the reactivity and efficacy of the nanoparticle in various applications, such as photocatalysis and antibacterial activity.

Furthermore, the data in Table 2 are used as input for the Rietveld refinement of ZnO-b NPs using Rietica software (Figure 4). This is a quantitative analysis that calculates cell parameters and requires the ZnO database model (No. 01-089-0510).

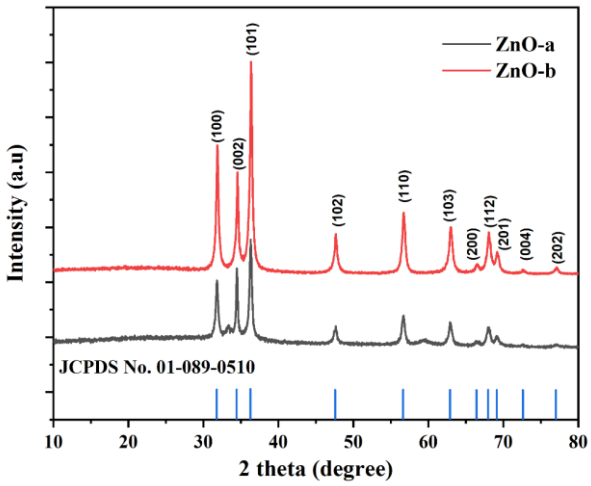

Figure 3. XRD pattern of ZnO NPs (λ = 1.5406 Å)

Table 2. Qualitative analysis results of the XRD pattern of ZnO NPs synthesized from *Cnidoscolus aconitifolius*

Phase/crystal structure	Space group	a (Å)	b (Å)	c (Å)	α (°)	β (°)	γ (°)
Zinc oxide/Hexagonal	P63 MC	3.252	3.252	5.2080	90	90	120

Table 3. Lattice parameter values of ZnO NPs after Rietveld refinement

Phase	Rietveld refinement				Shift of cell parameters			
	a (Å)	*b* (Å)	*c* (Å)	*V* (Å)	Δ*a* (Å)	Δ*b* (Å)	Δ*c* (Å)	Δ*V* (Å)
Zinc oxide	3.2519	3.2519	5.2079	46.89137	0.0321	0.0321	0.0064	0.880661

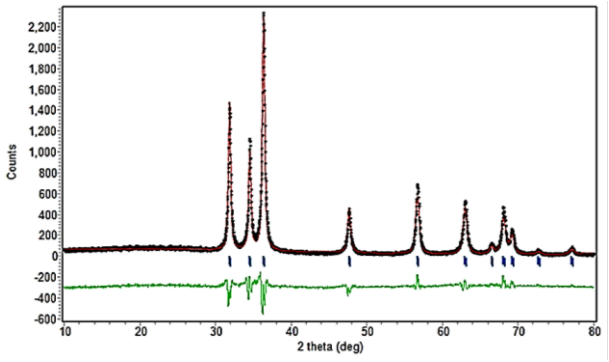

Figure 4. Refinement Rietveld of ZnO-b NPs

The refinement pattern is shown in Figure 4, with the color graph plot between the measured data pattern (black) and the calculated data pattern (red) overlapping considerably, indicating the suitability of the experimental data with the model data. The green pattern shows the difference (residual) between the experimental and simulation data. Quantitative analysis calculations using Rietica software yielded a suitability value indicating the degree of agreement between the experimental data and the model. The suitability of the two diffractogram patterns is evidenced by the R values (R_p, R_{wp}, R_{exp}, R_B, and Goodness-of-Fit (GoF)) in the refinement process, which are 12.56, 14.44, 9.72, 4.30, and 2.58.

The shift in lattice parameter values is presented in Table 3, indicating a corresponding change in the unit cell volume. Although the molar percentage of ZnO in the sample is small, the ZnO diffraction peaks remain sharp and distinct because: (1) ZnO possesses a stable wurtzite crystal structure that is maintained even under doping or compositional changes; (2) the wurtzite phase is highly crystalline, resulting in sharp diffraction peaks; and (3) Zn atoms have a high X-ray scattering coefficient, ensuring a significant contribution to the diffraction pattern even at low concentrations [30].

3.3. Morphology of ZnO NP

Micrograph (SEM) image of ZnO-b, obtained at 30 KX magnification (Figure 5). The morphology of the formed structure is predominantly nano-spherical, with an almost even diameter size distribution and uniform arrangement.

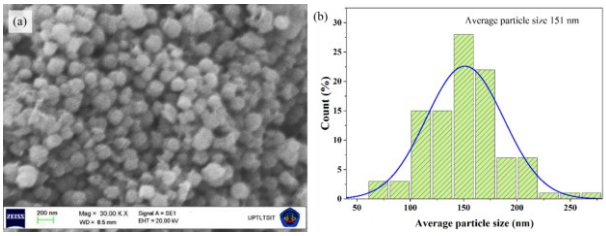

Figure 5. (a) SEM micrograph of ZnO-b synthesized using the biosynthesis method, scale bar 200 nm, and (b) Histogram of particle size ZnO-b

The zones in the nanospherical (Figure 5) confirm the presence of ZnO, as indicated by the qualitative XRD analysis (Table 2), suggesting that the sample produced through green synthesis is zinc oxide with a hexagonal phase and a crystalline structure. ImageJ software analysis yielded an average particle size distribution value of 151 nm (Figure 5). While the particle size seen from SEM (~151 nm) indicates the aggregation of several crystallites, the crystallite size of ZnO-b determined from XRD (17.64 nm) depicts the dimension of a single coherent crystalline domain. As a result, these two parameters are not directly comparable and describe distinct physical features. The ~151 nm particles observed in SEM correspond to agglomerated structures formed by several crystallites bound together, representing the overall morphology rather than an individual crystal domain.

3.4. Optical Properties of ZnO NPs

The absorbance spectrum and optical properties of ZnO NPs were observed using UV-visible spectroscopy, as shown in Figure 6. Using the Tauc plot formula (Equation 3), the energy band gap value was estimated from reflectance spectra data obtained using UV-DRS.

$$(\alpha h\upsilon)^{n} = A\left(h\upsilon - E_g\right) \quad (3)$$

Where, h, A, ν, E_g, are Planck's constant (Js), constant of proportionality (J), frequency (Hz), and band gap energy (eV), α is the absorption coefficient, n is a factor of the electron transition: direct transition (n = 2), and indirect transition (n = 1/2), respectively. A vigorous absorbance is observed at 333 and 357 nm (Figure 6a), within the measuring wavelength range 200-800 nm. These absorption peaks indicate the electron transition width and are used to estimate the band gap energy using Equation 3.

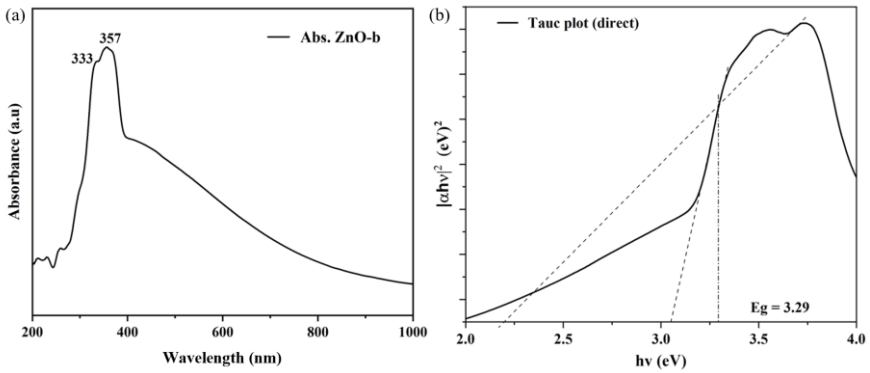

Figure 6. (a) UV-Vis DRS absorbance spectrum and (b) Tauc Plot, for nanoparticles ZnO-b

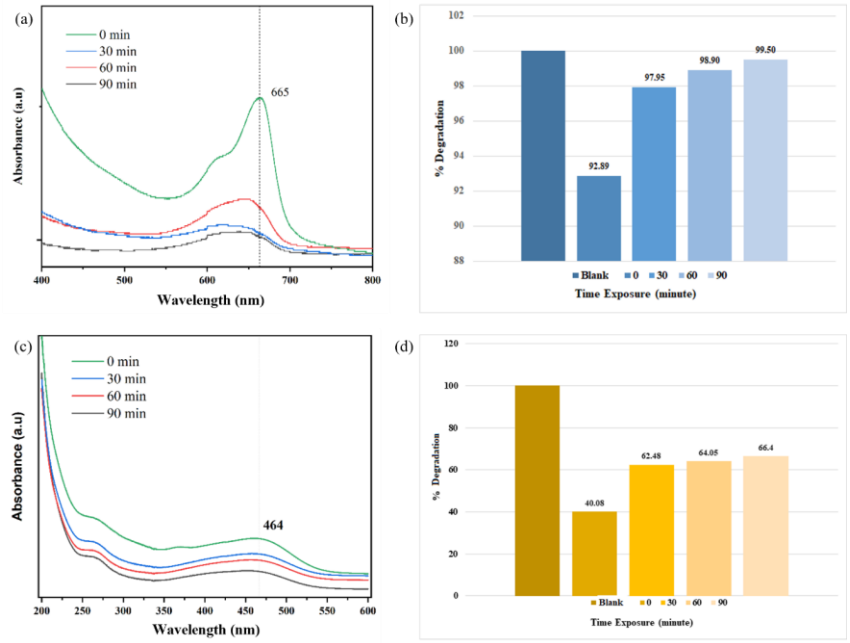

Figure 7. UV–Vis absorbance spectra and color changes of MB (a, b) and MO (c, d). The starting dye concentration (C_o) is indicated by the initial column (100%). The dye solution that was exposed to the same light conditions but without any catalyst is denoted as "Blank". Reaction conditions: 0.1 mg ZnO-b in 100 mL of MB and MO solutions, respectively

We estimated the band gap energy of the ZnO-b sample by plotting $(\alpha h\nu)^n$ against the photon energy ($h\nu$). The optical absorption coefficient was determined from the x-axis intercept of the linear region, as shown in Figure 6b. The resulting band gap of 3.29 eV aligns with the wavelength region effectively absorbed by the photocatalyst and is consistent with previous findings [31]. This value is slightly lower than the standard ZnO band gap (3.37 eV) but higher than the result reported in Suciyati *et al.* [18], likely due to the synthesis method, particularly the calcination step. The observed absorption peaks at 333 and 357 nm further confirm the formation of ZnO-b. The agreement between the ZnO-b absorption pattern and that of standard ZnO can be inferred from its overall band gap characteristics, even though the absorption wavelengths appear slightly shorter, which is typical for synthesized ZnO-b [32].

The optical band gap of ZnO-b (3.29 eV) suggests the absence of a quantum confinement effect, which is likely attributed to the relatively large particle size. The slight reduction in the E_g value may be associated with the presence of intrinsic defects such as oxygen vacancies and lattice strain, which can introduce localized states within the forbidden energy band. Furthermore, lattice distortion and the adsorption of organic residues during synthesis may also contribute to the narrowing of the band gap. Similar observations have been reported by several previous studies [33, 34, 35], showing that structural defects and crystal stress reduce the ZnO band gap. The obtained band gap energy (3.29 eV) confirms that the synthesized ZnO NPs are well-suited for photocatalytic applications, particularly for the absorption of UV-A light [31]. The presence of the ZnO phase is believed to enhance photocatalytic activity, enabling the efficient degradation of both cationic (MB) and anionic (MO) dyes.

Tests on MB and MO showed photo-degradation activity of cationic and anionic dyes, where, with an E_g of 3.29 eV, the ZnO-b photocatalyst could absorb UV-A light. MB and MO degradation were monitored at their maximum absorption peaks, 665 nm and 464 nm, respectively (Figure 7). The dye–catalyst mixture was stirred in the dark for 30 minutes to achieve adsorption–desorption equilibrium on the ZnO surface. The initial dye concentration (C_o = 100%) was used as a reference, and the relative concentration (C/C_o) during UV irradiation

was monitored to determine degradation efficiency. A blank dye solution without a catalyst was tested under identical conditions to evaluate the effects of photolysis and adsorption. Observations were conducted for 90 minutes, divided into 30-minute intervals, using a UV lamp (300 watts) as the light source. The photocatalyst (ZnO-b) was 0.1 g and was added to the MB solution (100 mL) and the MO solution (100 mL).

The photocatalytic activity of ZnO-b was swift after being irradiated by UV light. The spectrum in Figure 7 (a, c) shows the degradation activity of MB and MO for 90 minutes, indicating that the green-synthesized ZnO-b from *Chinosdolus aconitifolius* was very effective, especially for MB. Photocatalysis is a surface reaction that relies on the existence of an active surface area to facilitate the reaction. When correlated with the band gap of ZnO-b (3.29 eV), this gap is related to the recombination of electron-hole pairs, indicating the photocatalytic efficiency [36]. The absorbance data obtained by the UV-Vis Spectrometer decreased, and over 90 minutes of measurement, the data for MB and MO were 0.142, 0.041, 0.022, 0.010, and 0.305, 0.191, 0.183, 0.171, respectively. This decrease indicates a degradation efficiency of 92.96%, which is very high for ZnO-b performance on MB. While on MO, the efficiency was 43.93%, still higher than the research of Wang *et al.* [37].

The decrease in UV absorption intensity by ZnO-b is shown in Figure 7b. In this study, the effect of adding a ZnO-b catalyst (0.1 g) immediately after it was inserted into the MB solution, and before exposure to UV light, was observed to have degraded MB by 92.89%. The noticeable decline in dye density without UV light is attributed to dye sticking to the material, rather than pressure-based catalysis. The level of physical force generated by the magnetic stirrer is not strong enough to produce a noticeable electrical charge in the ZnO crystals, which typically require very high-frequency agitation. Hence, the observed process corresponds to adsorption–desorption equilibrium preceding photocatalytic degradation. Although ZnO inherently exhibits piezoelectric properties, substantial piezocatalytic activity is typically observed in anisotropic structures, such as nanorods or nanowires. In these anisotropic structures, mechanical pressure can generate a resultant polarization. Consequently, the almost round ZnO NPs created throughout this study are predicted to demonstrate a negligible piezoelectric impact when subjected to magnetic agitation.

The photocatalytic activity was maintained by exposing the sample to UV light for 90 minutes. The value of absorption was found to be 99.5% indicating that the absorption of UV light by ZnO-b was very adequate. The condition occurs because the absorption of high photon energy (~3.29 eV) and electron recombination are slow, resulting in efficient photocatalyst performance for dye degradation. The degradation efficiency of MB (92.96%) by ZnO-b is significantly higher than that in our previous studies [18], which proves that the addition of a calcination step in the synthesis has improved the performance of ZnO-b.

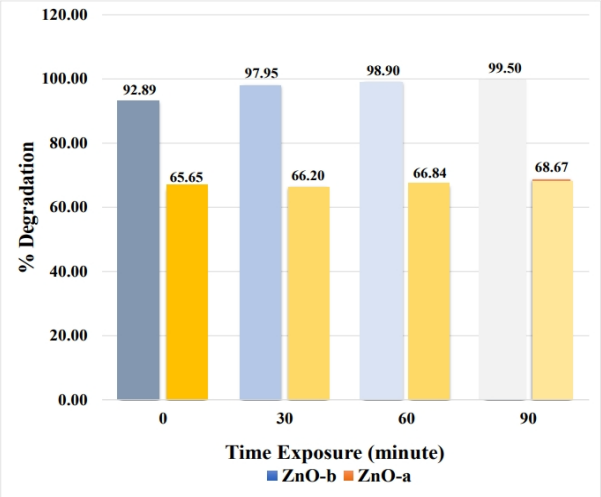

Figure 8. Photodegradation performance of ZnO-a (E_g = 2.97) and ZnO-b (E_g = 3.29)

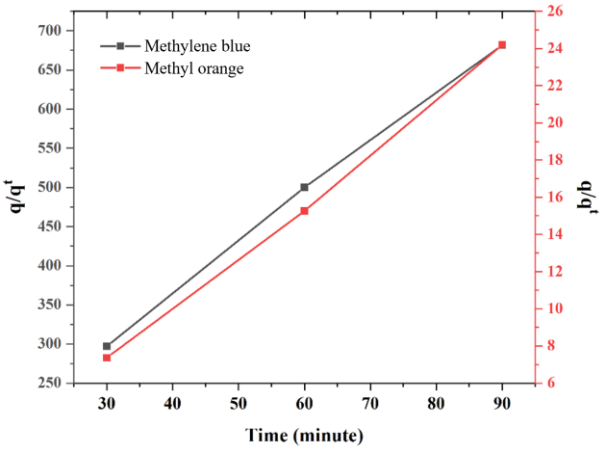

Figure 9. Pseudo-second-order kinetics model of MB (k_2 = 0.38 min^{-1}) and MO (k_2 = 0.064 min^{-1}) by using ZnO-b

Compared with our previous research [18], the variation in the band gap energy significantly affects the photocatalytic degradation of MB. As shown in Figure 8, ZnO-b exhibits superior photodegradation performance compared to ZnO-a. This enhancement can be attributed to the smaller particle size and improved crystal structure of ZnO-b, which together contribute to a larger specific surface area. A higher surface area provides more active sites for adsorbing dye molecules, thereby facilitating more efficient interaction between the photocatalyst and the substrate. Consequently, the increased availability of active sites promotes simultaneous photocatalytic reactions, thereby increasing the degradation rate of the MB dye [38].

Further quantitative evaluation using the pseudo-second-order kinetic model (k_2) indicated that surface adsorption on ZnO-b predominantly governed the overall reaction rate. The calculated rate constants (k_2) for the photocatalytic degradation of MB and MO were 0.38 min^{-1} and 0.064 min^{-1}, respectively, after 90 minutes of irradiation. These values are notably higher than those reported by Alprol *et al.* [39] for the unmodified ZnO, indicating the superior photocatalytic activity of ZnO-b. Despite the high degradation efficiency of 92.96% for MB

within 90 minutes, the overall kinetics were still influenced by the complex interactions between MB molecules and the active sites of the photocatalyst. In comparison, the degradation efficiency of MO reached approximately 43.93% under the same conditions. The corresponding rate constants for MB and MO degradation by ZnO-b are presented in Figure 9.

The breakdown kinetics of MO followed a pseudo-second-order model, suggesting that the adsorption surface of ZnO-b regulates the degradation process. The crucial role of surface interactions, involving dye molecules and the photocatalyst's active sites, is reflected in this k_2. Lending credence to the idea that adsorption is the rate-limiting step in this process. According to that kinetic model, the rate of the degradation process is determined by the adsorption of MO molecules onto the ZnO-b surface through chemisorption. The restricted electrostatic interaction between the negatively charged MO and the ZnO-b surface at a neutral pH is probably the cause of this circumstance [40]. Additionally, the effectiveness of these kinetics can be attributed to the advantageous crystalline structure of ZnO-b, the size of the nanoparticles, which allows for a larger surface area. However, more structural characterisation and reactivity experiments are required to confirm the primary mechanism at work. It should be noted that a direct comparison with previously reported degradation efficiencies for MB and MO is not provided, as the current work focuses primarily on the intrinsic photocatalytic behavior of the synthesized ZnO samples under controlled experimental conditions.

4. Conclusion

The green synthesis of ZnO NPs calcined at 250°C yields a pure zinc oxide phase with spherical shape and outstanding performance. Because the materials required for preparation are readily available and no surfactant or structure-directing agent is added, the preparation procedure is straightforward. The entire preparation procedure is quite environmentally beneficial. According to the FTIR patterns, the calcination process affects the degradation of functional groups, including amino and carboxylic groups, contained in the *Cnidoscolus aconitifolius* leaf extract, which helps stabilize the size of the nanoparticles. SEM micrographs confirm the uniformity of most of the grain sizes. The crystal structure of the ZnO-b has an average diameter of 17.24 nm, corresponding to the hexagonal wurtzite phase of ZnO, as confirmed by XRD analysis. The band gap energy of 3.29 eV, obtained from UV-Vis-DRS spectroscopy, suggests an association between oxygen vacancies and their impact on photocatalytic activity in ZnO-b materials. The photodegradation results reveal that ZnO-b exhibits high photocatalytic efficiencies, reaching 99.50% for methylene blue. Conversely, the degradation efficiencies for methyl orange were 60.40% under the same conditions, namely 90 minutes of UV exposure time. These observations suggest that optimizing parameters, such as pH and surface modification of ZnO-b, could further enhance its photocatalytic performance, particularly for the degradation of anionic dyes.

Acknowledgments

Thank you to the Institute for Research and Community Service, University of Lampung, for the funding provided through the Basic Research Grant with contract number 728/UN26.21/PN/2023. Thank you to the Material Physics Laboratory of the University of Lampung for the research implementation.

References

[1] Chin Boon Ong, Law Yong Ng, Abdul Wahab Mohammad, A review of ZnO nanoparticles as solar photocatalysts: Synthesis, mechanisms and applications, *Renewable and Sustainable Energy Reviews*, 81, (2018), 536-551 https://doi.org/10.1016/j.rser.2017.08.020

[2] Neha Srivastava, Manish Srivastava, P. K. Mishra, Vijai Kumar Gupta, *Green Synthesis of Nanomaterials for Bioenergy Applications*, John Wiley & Sons, 2020,

[3] Mohammad Raouf Hosseini, Mehdi Nasiri Sarvi, Recent achievements in the microbial synthesis of semiconductor metal sulfide nanoparticles, *Materials Science in Semiconductor Processing*, 40, (2015), 293-301 https://doi.org/10.1016/j.mssp.2015.06.003

[4] Mahmoud Nasrollahzadeh, Monireh Atarod, Mohaddeseh Sajjadi, S. Mohammad Sajadi, Zahra Issaabadi, Chapter 6 - Plant-Mediated Green Synthesis of Nanostructures: Mechanisms, Characterization, and Applications, in: M. Nasrollahzadeh, S.M. Sajadi, M. Sajjadi, Z. Issaabadi, M. Atarod (Eds.) *Interface Science and Technology*, Elsevier, 2019, https://doi.org/10.1016/B978-0-12-813586-0.00006-7

[5] Jagpreet Singh, Tanushree Dutta, Ki-Hyun Kim, Mohit Rawat, Pallabi Samddar, Pawan Kumar, 'Green' synthesis of metals and their oxide nanoparticles: applications for environmental remediation, *Journal of Nanobiotechnology*, 16, 1, (2018), 84 http://doi.org/10.1186/s12951-018-0408-4

[6] Parita Basnet, T. Inakhunbi Chanu, Dhrubajyoti Samanta, Somenath Chatterjee, A review on bio-synthesized zinc oxide nanoparticles using plant extracts as reductants and stabilizing agents, *Journal of Photochemistry and Photobiology B: Biology*, 183, (2018), 201-221 https://doi.org/10.1016/j.jphotobiol.2018.04.036

[7] Jaison Jeevanandam, Siaw Fui Kiew, Stephen Boakye-Ansah, Sie Yon Lau, Ahmed Barhoum, Michael K. Danquah, João Rodrigues, Green approaches for the synthesis of metal and metal oxide nanoparticles using microbial and plant extracts, *Nanoscale*, 14, 7, (2022), 2534-2571 http://doi.org/10.1039/D1NR08144F

[8] R. Yuvakkumar, J. Suresh, B. Saravanakumar, A. Joseph Nathanael, Sun Ig Hong, V. Rajendran, Rambutan peels promoted biomimetic synthesis of bioinspired zinc oxide nanochains for biomedical applications, *Spectrochimica Acta Part A: Molecular and Biomolecular Spectroscopy*, 137, (2015), 250-258 https://doi.org/10.1016/j.saa.2014.08.022

[9] S. Rajeshkumar, S. Venkat Kumar, Arunachalam Ramaiah, Happy Agarwal, T. Lakshmi, Selvaraj Mohana Roopan, Biosynthesis of zinc oxide nanoparticles using *Mangifera indica* leaves and

evaluation of their antioxidant and cytotoxic properties in lung cancer (A549) cells, *Enzyme and Microbial Technology*, 117, (2018), 91-95 https://doi.org/10.1016/j.enzmictec.2018.06.009

[10] Sri Wahyu Suciyati, Posman Manurung, Junaidi Junaidi, Rudy Situmeang, Optical and Crystal Structure Properties of ZnO Nanoparticle Synthesized through Biosynthesis Method for Photocatalysis Application, *Indonesian Journal of Chemistry*, 24, 1, (2024), 125-140 http://doi.org/10.22146/ijc.84796

[11] Morteza Golmohammadi, Moones Honarmand, Saeed Ghanbari, A green approach to synthesis of ZnO nanoparticles using jujube fruit extract and their application in photocatalytic degradation of organic dyes, *Spectrochimica Acta Part A: Molecular and Biomolecular Spectroscopy*, 229, (2020), 117961 https://doi.org/10.1016/j.saa.2019.117961

[12] Awanda Halida Ramadanti, Dina Kartika Maharani, Green synthesis of ZnO nanoparticles with papaya leaf extract (*Carica papaya* L.) as a reductor and its application on cotton fabrics, *Indonesian Journal of Chemical Science*, 11, 3, (2022), 198-206

[13] You-Kang Phang, Mohammod Aminuzzaman, Md. Akhtaruzzaman, Ghulam Muhammad, Sayaka Ogawa, Akira Watanabe, Lai-Hock Tey, Green Synthesis and Characterization of CuO Nanoparticles Derived from Papaya Peel Extract for the Photocatalytic Degradation of Palm Oil Mill Effluent (POME), *Sustainability*, 13, 2, (2021), 796 https://doi.org/10.3390/su13020796

[14] Demi Dama Yanti, Sintia Aprilia, Bambang Ariwahjoedi, Muhamad Allan Serunting, Hawa Purnama Celala Ary Cane, Biosynthesis of ZnO Nanoparticles Mediated by *Crescentia cujete* L Leaves Extract and The Photocatalytic Activities Towards Methylene Blue, *Jurnal Kimia Sains dan Aplikasi*, 26, 12, (2023), 457-465 https://doi.org/10.14710/jksa.26.12.457-465

[15] Milena María Ramírez Rodrigues, Jorge Carlos Metri Ojeda, Mariana González Díaz, Diana Karina Baigts Allende, Use of chaya (*Cnidoscolous chayamansa*) leaves for nutritional compounds production for human consumption, *Journal of the Mexican Chemical Society*, 65, 1, (2021), 118-128 https://doi.org/10.29356/jmcs.v65i1.1433

[16] Aarón Kuri-García, Jorge Luis Chávez-Servín, Salvador Horacio Guzmán-Maldonado, Phenolic profile and antioxidant capacity of *Cnidoscolus chayamansa* and *Cnidoscolus aconitifolius*: A review, *Journal of Medicinal Plants Research*, 11, 45, (2017), 713-727 http://doi.org/10.5897/JMPR2017.6512

[17] Javed Iqbal, Banzeer Ahsan Abbasi, Tabassum Yaseen, Syeda Anber Zahra, Amir Shahbaz, Sayed Afzal Shah, Siraj Uddin, Xin Ma, Blqees Raouf, Sobia Kanwal, Wajid Amin, Tariq Mahmood, Hamed A. El-Serehy, Parvaiz Ahmad, Green synthesis of zinc oxide nanoparticles using *Elaeagnus angustifolia* L. leaf extracts and their multiple in vitro biological applications, *Scientific Reports*, 11, 1, (2021), 20988 http://doi.org/10.1038/s41598-021-99839-z

[18] Sri Wahyu Suciyati, Junaidi Junaidi, Rudy Situmeang, Posman Manurung, Nano-ZnO prepared by using chaya and mango leaves extract for photocatalyst of methylene blue, *Journal of Metals, Materials and Minerals*, 34, 1, (2024), 1848 http://doi.org/10.55713/jmmm.v34i1.1848

[19] Luvedika Maheshwaran, Ladhurshika Nadarajah, S. P. N. N. Senadeera, C. B. Ranaweera, A. K. Chandana, R. N. Pathirana, Phytochemical Testing Methodologies and Principles for Preliminary Screening/ Qualitative Testing, *Asian Plant Research Journal*, 12, 5, (2024), 11–38 http://doi.org/10.9734/aprj/2024/v12i5267

[20] Xuan Thanh Tran, Thanh Thi Lan Bien, Thuan Van Tran, Thuy Thi Thanh Nguyen, Biosynthesis of ZnO nanoparticles using aqueous extracts of *Eclipta prostrata* and *Piper longum*: characterization and assessment of their antioxidant, antibacterial, and photocatalytic properties, *Nanoscale Advances*, 6, 19, (2024), 4885-4899 http://doi.org/10.1039/D4NA00326H

[21] Dipak Raj Jaishi, Indra Ojha, Govinda Bhattarai, Rabina Baraili, Ishwor Pathak, Dinesh Raj Ojha, Deepak Kumar Shrestha, Khaga Raj Sharma, Plant-mediated synthesis of zinc oxide (ZnO) nanoparticles using *Alnus nepalensis* D. Don for biological applications, *Heliyon*, 10, 20, (2024), https://doi.org/10.1016/j.heliyon.2024.e39255

[22] Tahani Saad Algarni, Naaser A. Y. Abduh, Abdullah Al Kahtani, Ahmed Aouissi, Photocatalytic degradation of some dyes under solar light irradiation using ZnO nanoparticles synthesized from *Rosmarinus officinalis* extract, *Green Chemistry Letters and Reviews*, 15, 2, (2022), 460-473 https://doi.org/10.1080/17518253.2022.2089059

[23] O. J. Nava, C. A. Soto-Robles, C. M. Gómez-Gutiérrez, A. R. Vilchis-Nestor, A. Castro-Beltrán, A. Olivas, P. A. Luque, Fruit peel extract mediated green synthesis of zinc oxide nanoparticles, *Journal of Molecular Structure*, 1147, (2017), 1-6 https://doi.org/10.1016/j.molstruc.2017.06.078

[24] C. A. Soto-Robles, P. A. Luque, C. M. Gómez-Gutiérrez, O. Nava, A. R. Vilchis-Nestor, E. Lugo-Medina, R. Ranjithkumar, A. Castro-Beltrán, Study on the effect of the concentration of *Hibiscus sabdariffa* extract on the green synthesis of ZnO nanoparticles, *Results in Physics*, 15, (2019), 102807 https://doi.org/10.1016/j.rinp.2019.102807

[25] Dorcas Mutukwa, Raymond Tichaona Taziwa, Lindiwe Khotseng, A Review of Plant-Mediated ZnO Nanoparticles for Photodegradation and Antibacterial Applications, *Nanomaterials*, 14, 14, (2024), 1182 https://doi.org/10.3390/nano14141182

[26] P. C. Nagajyothi, Sang Ju Cha, In Jun Yang, T. V. M. Sreekanth, Kwang Joong Kim, Heung Mook Shin, Antioxidant and anti-inflammatory activities of zinc oxide nanoparticles synthesized using *Polygala tenuifolia* root extract, *Journal of Photochemistry and Photobiology B: Biology*, 146, (2015), 10-17 https://doi.org/10.1016/j.jphotobiol.2015.02.008

[27] Afzal Hussain, Mohammad Oves, Mohamed F. Alajmi, Iqbal Hussain, Samira Amir, Jahangeer Ahmed, Md Tabish Rehman, Hesham R. El-Seedi, Imran Ali, Biogenesis of ZnO nanoparticles using *Pandanus odorifer* leaf extract: anticancer and antimicrobial activities, *RSC Advances*, 9, 27, (2019), 15357-15369 https://doi.org/10.1039/c9ra01659g

[28] A. Narayana, N. Azmi, M. Tejashwini, U. Shrestha, S. V. Lokesh, Synthesis and characterization of zinc

oxide (ZnO) nanoparticles using mango (*Mangifera indica*) leaves, *International Journal of Research and Analytical Reviews*, 5, 3, (2018), 432-439 http://doi.one/10.1729/Journal.18354

[29] Sanaz Alamdari, Morteza Sasani Ghamsari, Chan Lee, Wooje Han, Hyung-Ho Park, Majid Jafar Tafreshi, Hosein Afarideh, Mohammad Hosein Majles Ara, Preparation and Characterization of Zinc Oxide Nanoparticles Using Leaf Extract of *Sambucus ebulus*, *Applied Sciences*, 10, 10, (2020), 3620 https://doi.org/10.3390/app10103620

[30] Suresh Kumar, Divya Arora, Anu Dhupar, Vandana Sharma, J. K. Sharma, S. K. Sharma, Anurag Gaur, Structural and optical properties of polycrystalline ZnO nanopowder synthesized by direct precipitation technique, *Journal of Nano- and Electronic Physics*, 12, 4, (2020), 04027 https://doi.org/10.21272/jnep.12(4).04027

[31] Bachir Gherbi, Salah Eddine Laouini, Souhaila Meneceur, Abderrhmane Bouafia, Hadia Hemmami, Mohammed Laid Tedjani, Gobika Thiripuranathar, Ahmed Barhoum, Farid Menaa, Effect of pH Value on the Bandgap Energy and Particles Size for Biosynthesis of ZnO Nanoparticles: Efficiency for Photocatalytic Adsorption of Methyl Orange, *Sustainability*, 14, 18, (2022), 11300 https://doi.org/10.3390/su141811300

[32] Minha Naseer, Usman Aslam, Bushra Khalid, Bin Chen, Green route to synthesize Zinc Oxide Nanoparticles using leaf extracts of *Cassia fistula* and *Melia azadarach* and their antibacterial potential, *Scientific Reports*, 10, 1, (2020), 9055 http://doi.org/10.1038/s41598-020-65949-3

[33] Norlida Kamarulzaman, Muhd Firdaus Kasim, Roshidah Rusdi, Band Gap Narrowing and Widening of ZnO Nanostructures and Doped Materials, *Nanoscale Research Letters*, 10, 1, (2015), 346 http://doi.org/10.1186/s11671-015-1034-9

[34] Yuanshen Qi, Yaron Kauffmann, Anna Kosinova, Askar R. Kilmametov, Boris B. Straumal, Eugen Rabkin, Gradient bandgap narrowing in severely deformed ZnO nanoparticles, *Materials Research Letters*, 9, 1, (2021), 58-64 http://doi.org/10.1080/21663831.2020.1821111

[35] Milan Masar, Hassan Ali, Ali Can Guler, Michal Urbanek, Pavel Urbanek, Barbora Hanulikova, Hana Pistekova, Adriana Annusova, Michal Machovsky, Ivo Kuritka, Multifunctional bandgap-reduced ZnO nanocrystals for photocatalysis, self-cleaning, and antibacterial glass surfaces, *Colloids and Surfaces A: Physicochemical and Engineering Aspects*, 656, (2023), 130447 https://doi.org/10.1016/j.colsurfa.2022.130447

[36] S. K. Kansal, M. Singh, D. Sud, Studies on photodegradation of two commercial dyes in aqueous phase using different photocatalysts, *Journal of Hazardous Materials*, 141, 3, (2007), 581-590 https://doi.org/10.1016/j.jhazmat.2006.07.035

[37] Ying Wang, Chuanxi Yang, Yonglin Liu, Yuqi Fan, Feng Dang, Yang Qiu, Huimin Zhou, Weiliang Wang, Yuzhen Liu, Solvothermal Synthesis of ZnO Nanoparticles for Photocatalytic Degradation of Methyl Orange and p-Nitrophenol, *Water*, 13, 22, (2021), 3224 https://doi.org/10.3390/w13223224

[38] S. K. Pardeshi, A. B. Patil, Effect of morphology and crystallite size on solar photocatalytic activity of zinc oxide synthesized by solution free mechanochemical method, *Journal of Molecular Catalysis A: Chemical*, 308, 1, (2009), 32-40 https://doi.org/10.1016/j.molcata.2009.03.023

[39] Ahmed E. Alprol, Ahmed Eleryan, Ahmed Abouelwafa, Ahmed M. Gad, Tarek M. Hamad, Green synthesis of zinc oxide nanoparticles using *Padina pavonica* extract for efficient photocatalytic removal of methylene blue, *Scientific Reports*, 14, 1, (2024), 32160 https://doi.org/10.1038/s41598-024-80757-9

[40] Fan Zhang, Xin Chen, Fenghuang Wu, Yuefei Ji, High adsorption capability and selectivity of ZnO nanoparticles for dye removal, *Colloids and Surfaces A: Physicochemical and Engineering Aspects*, 509, (2016), 474-483 https://doi.org/10.1016/j.colsurfa.2016.09.059